Supporting ultrathin ZnIn2 S4 nanosheets on Co/N-doped graphitic carbon nanocages for efficient photocatalytic H2 generation

Wang, Sibo; Wang, Yan; Zhang, Song Lin; Zang, Shuang-Quan; Lou, David Xiong Wen

2019

Wang, S., Wang, Y., Zhang, S. L., Zang, S.-Q., & Lou, D. X. W. (2019). Supporting ultrathin ZnIn2 S4 nanosheets on Co/N-doped graphitic carbon nanocages for efficient photocatalytic H2 generation. Advanced Materials, 31(41), 1903404-. doi:10.1002/adma.201903404

https://hdl.handle.net/10356/138636

https://doi.org/10.1002/adma.201903404

Supporting Ultrathin $ZnIn_2S_4$ Nanosheets on Co/N-Doped Graphitic Carbon Nanocages for Efficient Photocatalytic H_2 Generation

*Sibo Wang, Yan Wang, Songlin Zhang, Shuang-Quan Zang and Xiong Wen (David) Lou**

[*] Dr. S. Wang, Y. Wang, S. L. Zhang, Prof. X. W. Lou

School of Chemical and Biomedical Engineering, Nanyang Technological University, 62 Nanyang Drive, Singapore 637459, Singapore

Email: xwlou@ntu.edu.sg; davidlou88@gmail.com

Webpage: http://www.ntu.edu.sg/home/xwlou/

Prof. S. Q. Zang

College of Chemistry and Molecular Engineering, Zhengzhou University, Henan 450001, P. R. China

Abstract

Ultrathin $ZnIn_2S_4$ nanosheets (NSs) have been grown on Co/NGC nanocages, composed of Co nanoparticles surrounded by few-layered N-doped graphitic carbon (NGC), to obtain hierarchical Co/NGC@$ZnIn_2S_4$ hollow heterostructures for photocatalytic H_2 generation with visible light. The photoredox functions of discrete Co, conductive NGC and $ZnIn_2S_4$ NSs are precisely combined into hierarchical composite cages possessing strongly hybridized shell and ultrathin layered substructures. Such structural and compositional virtues can expedite charge separation and mobility, offer large surface area and abundant reactive sites for water photosplitting. The Co/NGC@$ZnIn_2S_4$ photocatalyst exhibits outstanding H_2 evolution activity (e.g., 11270 μmol h^{-1} g^{-1}) and high stability without engaging any cocatalyst.

Keywords: hydrogen evolution, hollow structures, $ZnIn_2S_4$, N-doped carbon, photocatalysis

Employing photocatalysts to split water by solar energy for sustainable hydrogen production is intensively pursued by researchers.[1-3] Up to now, plenty of materials have been developed to catalyse the H_2 evolution reaction with significant progresses realized.[1-11] Nonetheless, the exploitation of efficient and stable H_2-releasing photocatalysts, particularly the materials independent of noble-metal cocatalysts (e.g., Pt), is still highly desirable, so as to drive this renewable fuel generation technology for practical application.

Mixed metal sulfides (e.g., $ZnIn_2S_4$) with layered structures have shown enormous potential for photocatalysis,[12-15] owing to the distinctive textural and photoelectronic properties. However, the single phase of metal sulfide nanosheets (NSs) typically evolve to bulky aggregates with modest activity and stability.[16] Assembling the metal sulfide NSs on preferred substrates to form composite photocatalysts can not only prevent them from aggregation but also render the benefits of heterojunction,[17-20] thus improving the efficiency of targeted reactions.

Graphitic carbon materials are widely used to composite with semiconductors to promote photocatalytic activity,[21-23] because of their high conductivity and superb electron mobility for directing the movement of charge carriers. Moreover, N-doping is believed to further strengthen the electronic and chemical features of carbonaceous materials to enhance photocatalytic efficiency.[22] On the other hand, cobalt species with smart electron-mediating ability are favorite moieties to make catalysts for photoredox reactions.[24-26] In particular, carbon-confined Co nanoparticles (NPs) have considerable potential for water splitting catalysis.[27-28] Besides tuning chemical compositions, designing proper structures for photocatalysts also strongly influences the catalytic performance.

Hollow structures are attracting intensive attention in various photocatalytic fields.[29] Hollow photocatalysts possess large surface area and plentiful reactive sites to enhance adsorption of reactants and boost surface-related redox reactions.[29-30] Meanwhile, the thin-shelled configuration of hollow scaffolds reduces charge diffusion length to assist separation and migration of electron-hole pairs.[31] Furthermore, hollow particles, especially polyhedral cages,[32] can enable reinforced

utilization of solar energy by the reflection/scattering effect inside the cavity.[33] Therefore, integrating all the aforementioned thoughts into one photocatalyst design is expected to achieve high efficiency for solar-driven H_2 production.

Herein, we grow ultrathin $ZnIn_2S_4$ NSs on Co/NGC nanocages with embedded Co NPs surrounded by a few-layered NGC shell to construct hierarchical Co/NGC@$ZnIn_2S_4$ (Co/NGC@ZIS) hollow heterostructures for photocatalytic water splitting to produce H_2. As illustrated in **Figure 1**, fabrication of the hierarchical hollow composites starts with zeolitic imidazolate framework-8 (ZIF-8) polyhedrons as the precursor to produce core-shell ZIF-8@ZIF-67 dodecahedrons through an in situ solution growth method. Then, the ZIF-8@ZIF-67 particles are treated by high-temperature pyrolysis and acid leaching, generating the Co/NGC nanocages. At last, ultrathin ZnI_2S_4 NSs are successfully grown on these Co/NGC nanocages to create hierarchical Co/NGC@ZIS cages. The catalytic functions of isolated Co NPs, conductive NGC and layered $ZnIn_2S_4$ are integrated into hierarchical hollow structures with tightly coupled heterogeneous shell and ultrathin sheet-like subunits. The unique structure and composition of Co/NGC@ZIS can facilitate charge separation and mobility, offer large surface area and abundant active sites to drive water photosplitting. As a result, the optimized Co/NGC@ZIS photocatalyst exhibits cocatalyst-free H_2 generation activity of 11270 μmol h^{-1} g^{-1} and high stability under visible light irradiation.

Highly uniform ZIF-8 polyhedrons are synthesized through a modified monodentate ligand-assisted approach (Figure S1, see Supporting Information).[34] The formation of ZIF-8 is confirmed by powder X-ray diffraction (XRD) and energy-dispersive X-ray (EDX) tests (Figure S2). The ZIF-8 particles are then mixed with $Co(NO_3)_2 \cdot 6H_2O$ and 2-methylimidazole in methanol and kept at room temperature to grow a ZIF-67 shell.[35] After the reaction, a purple ZIF-8@ZIF-67 core-shell product is harvested (Figure S3). The hybrid ZIFs particles show a similar dodecahedral structure with high uniformity and smooth surface (Figure S4). Afterward, the ZIF-8@ZIF-67 material is annealed at 800 °C in N_2 to convert to pristine Co/N-doped graphitic carbon (p-Co/NGC)

nanocages. XRD pattern of p-Co/NGC is indexed to metallic Co (JCPDS card no.: 89-7093) and graphitic carbon (Figure S5a). EDX analysis verifies the formation of p-Co/NGC composite made of Co, C and N elements (Figure S5b). The content of Co in p-Co/NGC is about 17.1 wt% determined by inductively coupled plasma optical emission spectrometry (ICP-OES). The p-Co/NGC particles (**Figure 2**a,b) well inherit the polyhedral morphology of the dual ZIF precursor. The closer FESEM studies indicate the slightly distorted surface of the rhombic dodecahedrons with obvious interior void (Figure S6a,b). The well-defined cage-shaped structure of p-Co/NGC is confirmed by TEM images (Figure 2c and Figure S6c,d). Besides, some large Co particles are observed in p-Co/NGC, which are thought to be charge recombination centers for photocatalysis and thus removed by acid etching.

The acid-treated Co/N-doped graphitic carbon (Co/NGC) material keeps the original phases of metallic Co and graphitic carbon (Figure S7a,b), and the Co content reduces to about 14.1 wt% determined by ICP-OES. The Raman spectrum of Co/NGC shows two peaks at 1337 and 1580 cm^{-1}, signifying the characteristic D and G bands of graphitic carbon (Figure S7c).[28] X-ray photoelectron spectroscopy (XPS) analysis confirms the elemental composition (i.e., Co, N and C) of Co/NGC and the metallic state of cobalt (Figure S8a,b). In addition, the N 1s and C 1s XPS spectra evidence that N is doped into the graphitic carbon (Figure S8c,d). The Co/NGC material is shown to be highly porous with a specific surface area of 518 $m^2 g^{-1}$ (Figure S9). The FESEM images reveal that Co/NGC particles preserve the dodecahedral structure after the acid treatment (Figure 2d,e and Figure S10a-d). Unlike the p-Co/NGC, no bulky Co particles are observed in Co/NGC (Figure 2f and Figure S10e). Further TEM analyses display that ultrasmall Co NPs with particle size of about 5 nm exist in Co/NGC (Figure 2g and Figure S10f). The high-resolution TEM (HRTEM) images exhibit clear crystal lattice with an interlayer distance of 0.20 nm (Figure 2h and Figure S10g-k), corresponding to (111) planes of metallic Co. Moreover, it is also discerned that the Co NPs are encapsulated in few-layered NGC shells with an interlayer spacing of 0.34 nm. Elemental mappings

of a single Co/NGC nanocage indicate the uniform distribution of Co, C and N in the entire particle (Figure 2i).

After the solvothermal reaction, an outer shell of $ZnIn_2S_4$ NSs is grown on each Co/NGC nanocage (**Figure 3**a and Figure S11a), producing the Co/NGC@ZIS heterostructures (Figure S12). The Co/NGC@ZIS particles show the polyhedral morphology with hierarchical surface constructed by building blocks of ultrathin $ZnIn_2S_4$ NSs (Figure 3b,c). The hierarchical hollow architecture of Co/NGC@ZIS is verified by TEM observation (Figure 3d,e, and Figure S11b). The HRTEM image of the outer NSs gives visible lattice fringes attributed to (102) crystal plane of hexagonal $ZnIn_2S_4$ (Figure S11c-f). The detailed TEM analysis on the shell of a Co/NGC@ZIS particle finds no perceptible interlayer gaps (Figure 3f), indicating the intimate adhesion between the inner Co/NGC nanocage and the outer $ZnIn_2S_4$ shell. The strong interaction is further revealed by the obvious binding energy shift in the Co 2p XPS spectra (Figure S13). Elemental mappings of Co/NGC@ZIS cages show that Co, N and C are distributed in interior edge of the shell, while Zn, In and S exist in the exterior region (Figure 3g). The synthetic method is advantageous to tune the composition of Co/NGC@ZIS by controlling the amount of Co/NGC. Two other samples, namely Co/NGC(2)@ZIS (Figures S14 and S15) and Co/NGC(8)@ZIS (Figures S16 and S17), are synthesized as two control samples to study the structure-composition-performance relationship. ICP-OES tests indicate that the Co contents of Co/NGC(2)@ZIS, Co/NGC@ZIS and Co/NGC(8)@ZIS are about 2.4, 4.6 and 6.3 wt%, respectively. In addition, hierarchical solid polyhedrons of Co/NGC@ZIS-S (Figures S18 and S19) and NGC@ZIS-S (Figures S20 and S21), hierarchical Co_3O_4/NGC@ZIS cages (Figures S22 and S23), and NS-assembled $ZnIn_2S_4$ particles (Figures S24 and S25) are also synthesized under similar conditions for comparison.

The hierarchical Co/NGC@ZIS hybrid cages show increased visible light absorption than the solid counterpart Co/NGC@ZIS-S (Figure S26), which may be attributed to the multi-light reflection in the cavity of the hollow polyhedrons.[32] The enhanced optical harvesting of

Co/NGC@ZIS will contribute to its photocatalytic performance. To study the redox potentials of Co/NGC@ZIS, UV photoelectron spectroscopy (UPS) tests are conducted. The Fermi levels (E_F) of Co/NGC and $ZnIn_2S_4$ are determined to be -0.07 and -0.14 V (*vs.* standard hydrogen electrode, SHE), respectively (Figure S27a,b). By combining the results of the XPS valance band (VB) spectrum and bandgap energy (E_g) of $ZnIn_2S_4$ (Figure S27c,d), its conduction band (CB) and VB positions are defined at -0.98 and 1.12 V (*vs.* SHE). Therefore, it is thermodynamically favorable for the photoinduced electrons on CB of $ZnIn_2S_4$ to transfer to E_F of Co/NGC for running the H_2 evolution reaction (Figure S28). N_2 sorption measurements confirm the presence of mesopores in Co/NGC@ZIS with high specific surface area of 180 m^2 g^{-1} and total pore volume of 0.36 cm^3 g^{-1} (Figure S29), which are much higher than that of $ZnIn_2S_4$ NS-assembled particles (Figure S30). The enhanced surface area and pore volume of Co/NGC@$ZnIn_2S_4$ indicate that the sample should possess more reactive site to promote heterogeneous redox reactions.[36] These results point to the opportunity of Co/NGC@ZIS for operating water splitting by visible light excitation.

Photocatalytic H_2 evolution reactions are evaluated in a cocatalyst-free system under visible light irradiation with triethanolamine as a hole scavenger. The bare Co/NGC nanocages are nearly inactive for catalyzing the H_2 production reaction (**Figure 4**a). Strikingly, after coupled with $ZnIn_2S_4$ NSs, the Co/NGC@ZIS hybrid manifests a remarkable H_2-liberating rate of 11270 μmol h^{-1} g^{-1}, which is also greatly higher than that of $ZnIn_2S_4$ NS-assembled particles (i.e., 2160 μmol h^{-1} g^{-1}). The H_2 evolution activity of Co/NGC@ZIS is comparable or higher to those of recent works (Table S1). The Co/NGC@ZIS photocatalyst affords a high apparent quantum efficiency (AQE) of 5.07 % at monochromatic light irradiation of 420 nm without using Pt as the cocatalyst.[3, 9, 37-38] Such findings highlight that supporting ultrathin $ZnIn_2S_4$ NSs on the Co/NGC nanocages forming hierarchical hollow heterostructures greatly improves the H_2 evolution efficiency. In comparison, the p-Co/NGC@ZIS sample exhibits much lower activity for the reaction, which should be mainly

due to the bulky Co particles in p-Co/NGC acting as recombination centers of photoinduced charge carriers.

As shown in Figure 4b, the hierarchical Co/NGC(2)@ZIS and Co/NGC(8)@ZIS cages show obviously inferior H_2 evolution performance compared to the Co/NGC@ZIS cages, which suggests that the composition of the heterostructure largely influences the catalytic efficiency. Furthermore, the hierarchical solid polyhedrons of Co/NGC@ZIS-S catalyze a H_2-yielding rate of 4580 μmol h^{-1} g^{-1}, substantially lower than that of Co/NGC@ZIS, which indicates the importance of hollow structure to the reaction. The control experiment using Co_3O_4/NGC@ZIS as the photocatalyst manifests markedly reduced activity compared to Co/NGC@ZIS. On the other hand, the photocatalytic performance of the NGC@ZIS-S solid particles is also much poorer than that of the Co/NGC@ZIS-S counterpart. These results imply that the water reduction reaction mainly occurs on the Co nanoparticles. The time course studies display that Co/NGC@ZIS enables a robust H_2 release activity for 6 h (Figure 4c), reaching a total yield of 70900 μmol g^{-1}, which significantly outperforms the individual components. The stability of Co/NGC@ZIS is then checked by the long-time activity tests for 20 h. There is no evident decrease in the reaction rates of successive five cycles (Figure 4d), suggesting high stability of the catalyst. Besides, XRD and TEM tests of the Co/NGC@ZIS sample after the H_2 evolution reaction also verify the high structural stability of the photocatalyst (Figure S31). The photocatalytic nature of the H_2 evolution reaction is revealed by activity evaluation under photoirradiation of different wavelengths (Figure S32). The variation tendency of H_2 formation matches well with the absorption spectrum, indicating the water reduction reaction is driven by light excitation.[37]

To understand the superior performance of Co/NGC@ZIS, photoelectrochemical (PEC) characterizations are performed. The steady-state photoluminescence (PL) spectra display obvious PL quenching of Co/NGC@ZIS compared to $ZnIn_2S_4$ (**Figure 5**a), indicating the restrained recombination of photoinduced charges.[39] Meanwhile, the time-resolved PL (TRPL) spectra show

that Co/NGC@ZIS exhibits a shorter average PL lifetime than $ZnIn_2S_4$ (i.e., 1.62 ns *vs.* 2.46 ns, Figure 4b). The apparent PL quenching and lifetime diminution indicate the efficient charge movement from $ZnIn_2S_4$ to Co/NGC in Co/NGC@ZIS.[13] Moreover, the electrochemical impedance spectra (EIS) show a smaller high-frequency semicircle in the Nyquist plot of Co/NGC@ZIS (Figure 5c), suggesting its reduced charge-transport resistance. Correspondingly, the transient photocurrent generation of Co/NGC@ZIS is also much enhanced (Figure 5d), reflecting the promoted charge transfer in the hybrid. These PEC results reveal the inhibited recombination and improved transport of charge carriers in Co/NGC@ZIS, thus ensuring the high H_2-evoluting efficiency. Based on the results of activity evaluation and PEC tests, one possible photocatalytic mechanism of the H_2 evolution reaction is proposed (Figure S28). Under visible light irradiation, the electrons on the VB of $ZnIn_2S_4$ are excited to its CB. Due to the energy difference between the E_F of $ZnIn_2S_4$ and Co/NGC, the photoinduced electrons on CB of $ZnIn_2S_4$ will migrate favorably to Co/NGC for generating H_2. Simultaneously, the photogenerated holes on VB of $ZnIn_2S_4$ initiate the oxidation reaction. In the Co/NGC@ZIS photocatalyst, the highly porous NGC shells with excellent charge mobility can effectively mediate electron transfer from $ZnIn_2S_4$ to the active Co sites for the H_2 evolution reaction.

In summary, ultrathin $ZnIn_2S_4$ nanosheets are grown on Co/NGC nanocages consisting of Co nanoparticles encapsulated in few-layered N-doped graphitic carbon (NGC), to form hierarchical Co/NGC@$ZnIn_2S_4$ cages for efficient photocatalytic H_2 generation. The template-engaged synthetic strategy can readily tune the structure and composition of the targeted material. The hollow composites with strongly hybridized shell and ultrathin layered substructures can offer abundant catalytic sites and boost charge separation and transfer. As a result, the optimized photocatalyst shows excellent activity and high stability for splitting water to generate H_2 in the absence of any cocatalysts. This work may inspire the design of semiconductor assemblies for high-efficiency solar-to-hydrogen fuel conversion.

Acknowledgements

X. W. L. acknowledges the funding support from the National Research Foundation (NRF) of Singapore via the NRF investigatorship (NRF-NRFI2016-04) and the Ministry of Education of Singapore through Academic Research Fund (AcRF) Tier-1 Funding (M4011783, RG5/17 (S)).

References

[1] S. Chen, T. Takata, K. Domen, *Nat. Rev. Mater.* **2017**, *2*, 17050.

[2] R. Kuriki, T. Ichibha, K. Hongo, D. Lu, R. Maezono, H. Kageyama, O. Ishitani, K. Oka, K. Maeda, *J. Am. Chem. Soc.* **2018**, *140*, 6648.

[3] Y. Xiao, G. Tian, W. Li, Y. Xie, B. Jiang, C. Tian, D. Zhao, H. Fu, *J. Am. Chem. Soc.* **2019**, *141*, 2508.

[4] Q. Wang, T. Hisatomi, Q. Jia, H. Tokudome, M. Zhong, C. Wang, Z. Pan, T. Takata, M. Nakabayashi, N. Shibata, Y. Li, I. D. Sharp, A. Kudo, T. Yamada, K. Domen, *Nat. Mater.* **2016**, *15*, 611.

[5] M. Liu, Y. Chen, J. Su, J. Shi, X. Wang, L. Guo, *Nat. Energy* **2016**, *1*, 16151.

[6] M. F. Kuehnel, C. E. Creissen, C. D. Sahm, D. Wielend, A. Schlosser, K. L. Orchard, E. Reisner, *Angew. Chem. Int. Ed.* **2019**, *58*, 5059.

[7] D. Zhong, W. Liu, P. Tan, A. Zhu, Y. Liu, X. Xiong, J. Pan, *Appl. Catal. B Environ.* **2018**, *227*, 1.

[8] Z. Zhang, Z. Zhao, Y. Hou, H. Wang, X. Li, G. He, M. Zhang, *Angew. Chem. Int. Ed.* **2019**, *58*, 8862.

[9] B. Lin, G. Yang, L. Wang, *Angew. Chem. Int. Ed.* **2019**, *58*, 4587.

[10] R. Chen, Z.-H. Yan, X.-J. Kong, L.-S. Long, L.-S. Zheng, *Angew. Chem. Int. Ed.* **2018**, *57*, 16796.

[11] H. Li, Y. Sun, Z. Y. Yuan, Z. Y. Pei, T. Y. Ma, *Angew. Chem. Int. Ed.* **2018**, *57*, 3222.

[12] S. Zhang, X. Liu, C. Liu, S. Luo, L. Wang, T. Cai, Y. Zeng, J. Yuan, W. Dong, Y. Pei, Y. Liu, *ACS Nano* **2018**, *12*, 751.

[13] M. Q. Yang, Y. J. Xu, W. Lu, K. Zeng, H. Zhu, Q. H. Xu, G. W. Ho, *Nat. Commun.* **2017**, *8*, 14224.

[14] X. Jiao, Z. Chen, X. Li, Y. Sun, S. Gao, W. Yan, C. Wang, Q. Zhang, Y. Lin, Y. Luo, Y. Xie, *J. Am. Chem. Soc.* **2017**, *139*, 7586.

[15] S. Wang, B. Y. Guan, X. Wang, X. W. Lou, *J. Am. Chem. Soc.* **2018**, *140*, 15145.

[16] Z. Chen, D. Li, W. Zhang, C. Chen, W. Li, M. Sun, Y. He, X. Fu, *Inorg. Chem.* **2008**, *47*, 9766.

[17] B. Xu, P. He, H. Liu, P. Wang, G. Zhou, X. Wang, *Angew. Chem. Int. Ed.* **2014**, *53*, 2339.

[18] J. Low, J. Yu, M. Jaroniec, S. Wageh, A. A. Al-Ghamdi, *Adv. Mater.* **2017**, *29*, 1601694.

[19] J. Ran, W. Guo, H. Wang, B. Zhu, J. Yu, S. Z. Qiao, *Adv. Mater.* **2018**, *30*, 1800128.

[20] W. Zeng, Y. Bian, S. Cao, Y. Ma, Y. Liu, A. Zhu, P. Tan, J. Pan, *ACS Appl. Mater. Interfaces* **2018**, *10*, 21328.

[21] Y.-X. Pan, Y. You, S. Xin, Y. Li, G. Fu, Z. Cui, Y.-L. Men, F.-F. Cao, S.-H. Yu, J. B. Goodenough, *J. Am. Chem. Soc.* **2017**, *139*, 4123.

[22] S. Wang, B. Y. Guan, X. W. Lou, *Energy Environ. Sci.* **2018**, *11*, 306.

[23] Q. Xiang, J. Yu, M. Jaroniec, *Chem. Soc. Rev.* **2012**, *41*, 782.

[24] S. Wang, B. Y. Guan, Y. Lu, X. W. Lou, *J. Am. Chem. Soc.* **2017**, *139*, 17305.

[25] P. Huang, J. Huang, S. A. Pantovich, A. D. Carl, T. G. Fenton, C. A. Caputo, R. L. Grimm, A. I. Frenkel, G. Li, *J. Am. Chem. Soc.* **2018**, *140*, 16042.

[26] S. Wang, B. Y. Guan, X. W. Lou, *J. Am. Chem. Soc.* **2018**, *140*, 5037.

[27] K. Zhang, J. Ran, B. Zhu, H. Ju, J. Yu, L. Song, S.-Z. Qiao, *Small* **2018**, *14*, 1801705.

[28] Y. Hou, Z. Wen, S. Cui, S. Ci, S. Mao, J. Chen, *Adv. Funct, Mater.* **2015**, *25*, 872.

[29] M. Xiao, Z. Wang, M. Lyu, B. Luo, S. Wang, G. Liu, H.-M. Cheng, L. Wang, *Adv. Mater.* **2018**, DOI: 10.1002/adma.201801369.

[30] P. Zhang, S. Wang, B. Y. Guan, X. W. Lou, *Energy Environ. Sci.* **2019**, *12*, 164.

[31] Y. Li, X. Cheng, X. Ruan, H. Song, Z. Lou, Z. Ye, L. Zhu, *Nano Energy* **2015**, *12*, 775.

[32] B. Qiu, Q. Zhu, M. Du, L. Fan, M. Xing, J. Zhang, *Angew. Chem. Int. Ed.* **2017**, *56*, 2684.

[33] J. Sun, J. Zhang, M. Zhang, M. Antonietti, X. Fu, X. Wang, *Nat. Commun.* **2012**, *3*, 1139.

[34] P. Zhang, B. Y. Guan, L. Yu, X. W. Lou, *Chem* **2018**, *4*, 162.

[35] Y. Pan, K. Sun, S. Liu, X. Cao, K. Wu, W.-C. Cheong, Z. Chen, Y. Wang, Y. Li, Y. Liu, D. Wang, Q. Peng, C. Chen, Y. Li, *J. Am. Chem. Soc.* **2018**, *140*, 2610.

[36] X. Wang, K. Maeda, X. Chen, K. Takanabe, K. Domen, Y. Hou, X. Fu, M. Antonietti, *J. Am. Chem. Soc.* **2009**, *131*, 1680.

[37] Z. Luo, Y. Fang, M. Zhou, X. Wang, *Angew. Chem. Int. Ed.* **2019**, *58*, 6033.

[38] W. Huang, Q. He, Y. Hu, Y. Li, *Angew. Chem. Int. Ed.* **2019**, *58*, 8676.

[39] H. Zhang, P. Zhang, M. Qiu, J. Dong, Y. Zhang, X. W. Lou, *Adv. Mater.* **2019**, *31*, 1804883.

Figures and Captions

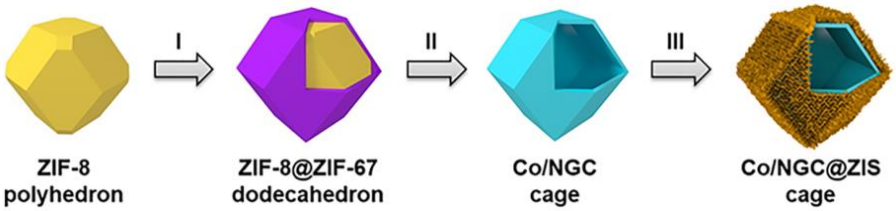

Figure 1. Schematic illustration for the synthetic process of hierarchical Co/NGC@ZIS cages. I: growth of ZIF-67 on ZIF-8 particles. II: carbonization in N_2 and acid etching. III: growth of $ZnIn_2S_4$ NSs.

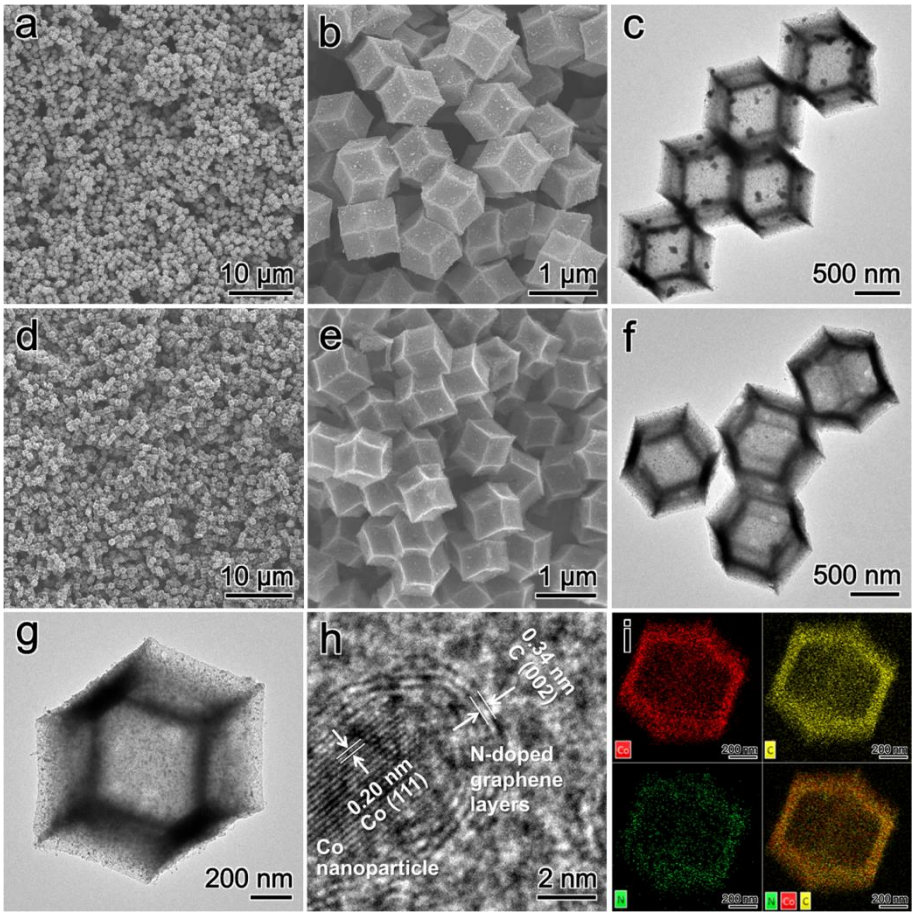

Figure 2. (a,b) FESEM images and (c) TEM image of p-Co/NGC nanocages. (d,e) FESEM images, (f,g) TEM images, (h) HRTEM image, and (i) elemental mappings of Co/NGC nanocages.

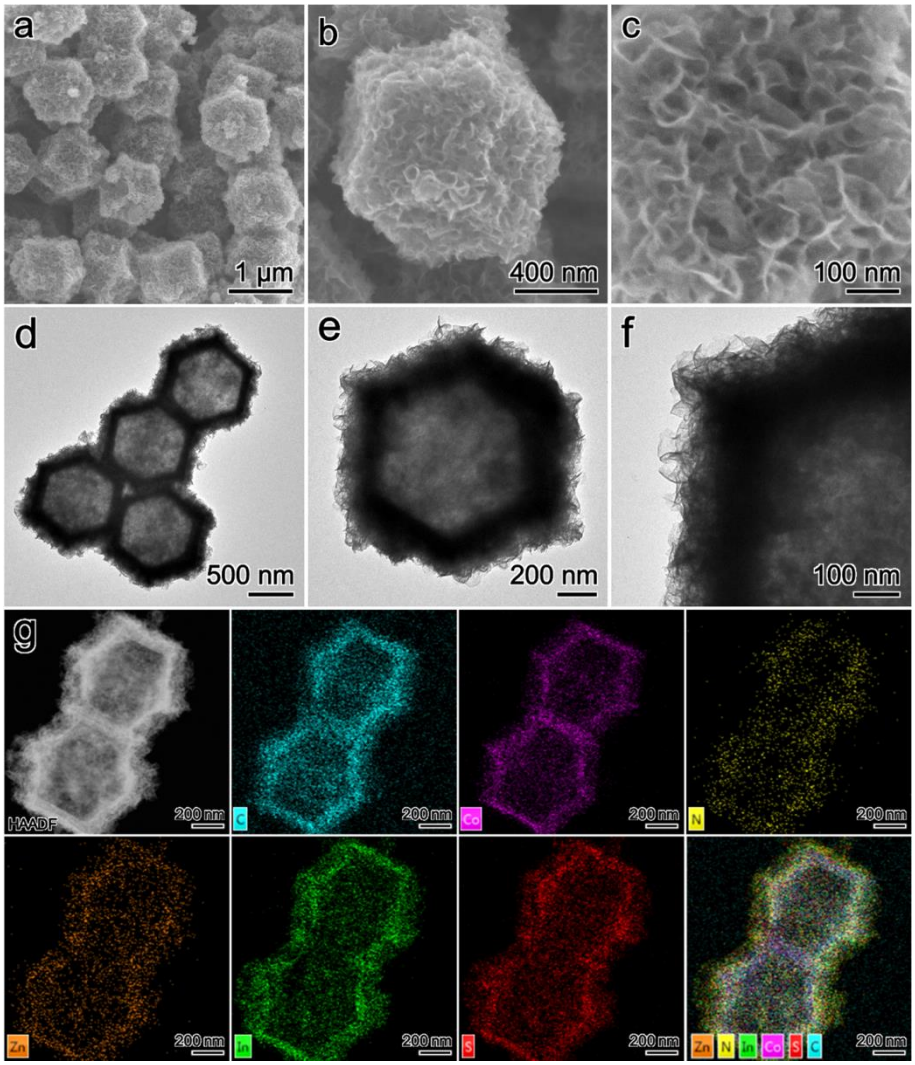

Figure 3. (a-c) FESEM images, (d-f) TEM images and (g) elemental mappings of hierarchical Co/NGC@ZIS cages.

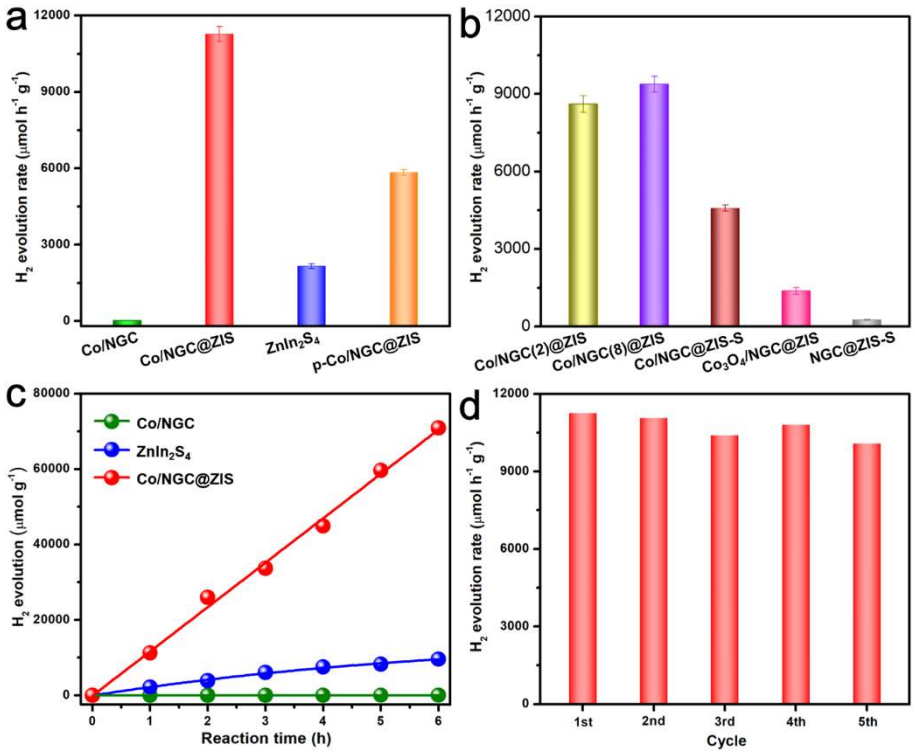

Figure 4. (a) Photocatalytic H_2 evolution activities of Co/NGC, Co/NGC@ZIS, $ZnIn_2S_4$ and p-Co/NGC@ZIS. (b) H_2 production rates of Co/NGC@ZIS with varied compositions, the solid counterparts of Co/NGC@ZIS-S and NGC@ZIS-S, and Co_3O_4/NGC@ZIS. (c) Time-yield plots of different samples. (d) H_2 yield rates of Co/NGC@ZIS in every 4 h reaction for successive five cycles.

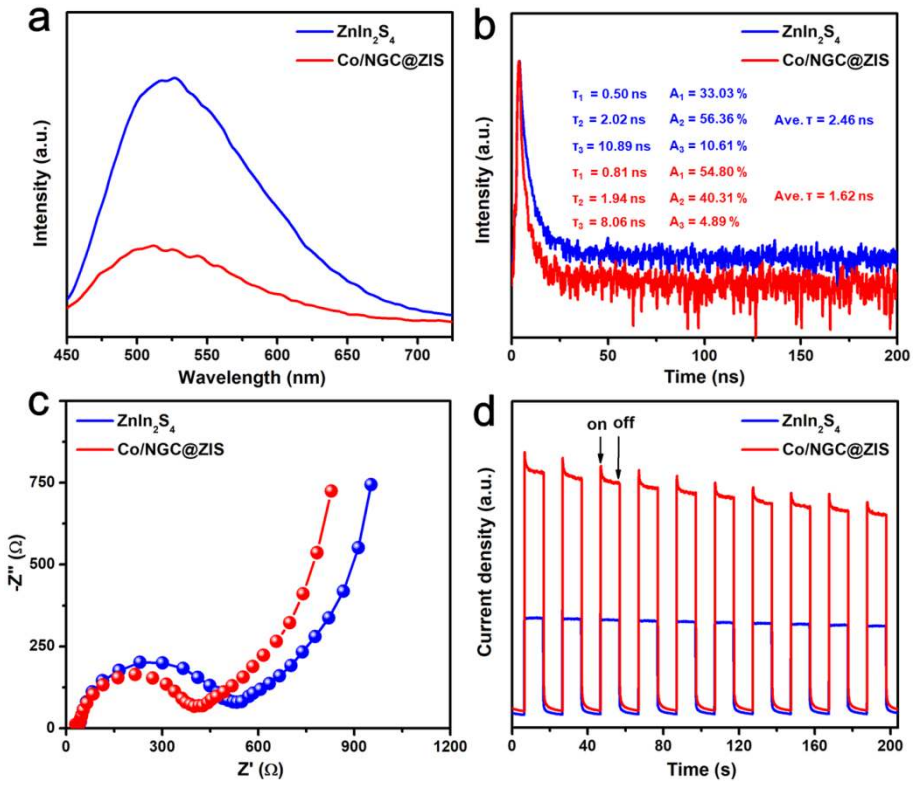

Figure 5. (a) Steady-state PL spectra, (b) TRPL spectra, (c) EIS spectra, and (d) transient photocurrent spectra of Co/NGC@ZIS and $ZnIn_2S_4$.

for Table of Content Entry

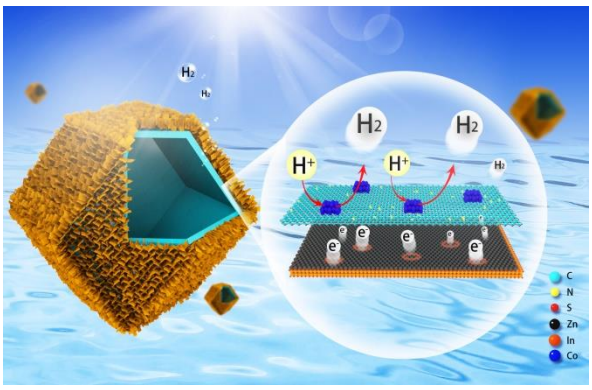

Hierarchical Co/NGC@$ZnIn_2S_4$ heterostructured cages are fabricated by supporting ultrathin $ZnIn_2S_4$ nanosheets on Co/N-doped graphitic carbon (Co/NGC) nanocages. This delicate design can facilitate charge separation and transport as well as provide large surface area and rich active sites for water photosplitting reactions. Outstanding activity and high stability for H_2 evolution under visible light are achieved without the assistance of any cocatalysts.